Letter

Disorder in dissipation-induced topological states: Evidence for a different type of localization transition

Alon Beck and Moshe Goldstein
Raymond and Beverly Sackler School of Physics and Astronomy, Tel Aviv University, Tel Aviv 6997801, Israel

(Received 26 November 2020; revised 5 April 2021; accepted 17 May 2021; published 1 June 2021)

The quest for nonequilibrium quantum phase transitions is often hampered by the tendency of driving and dissipation to give rise to an effective temperature, resulting in classical behavior. Could this be different when the dissipation is engineered to drive the system into a nontrivial quantum coherent steady state? In this work we shed light on this issue by studying the effect of disorder on recently introduced dissipation-induced Chern topological states, and examining the eigenmodes of the Hermitian steady-state density matrix or entanglement Hamiltonian. We find that, similarly to equilibrium, each Landau band has a single delocalized level near its center. However, using three different finite-size scaling methods we show that the critical exponent ν describing the divergence of the localization length upon approaching the delocalized state is significantly different from equilibrium if disorder is introduced into the nondissipative part of the dynamics. This indicates a different type of nonequilibrium quantum critical universality class accessible in cold-atom experiments.

DOI: 10.1103/PhysRevB.103.L241401

Introduction. Recent years have seen a surge of interest in the driven-dissipative dynamics of quantum many-body systems [1,2]. Of particular interest is the possibility of new nonequilibrium quantum critical phenomena. However, typically far-from-equilibrium conditions give rise to an effective temperature governing the long time physics, and leading to classical criticality. This stands in line with the usual perception of driving and dissipation as causing decoherence and destroying subtle quantum phenomena. This point of view has been challenged by recent works showing how coupling to an environment could be engineered to drive a system towards desired steady states displaying quantum correlations [3–9], such as nonequilibrium topological states [10–23]. In particular, Refs. [18,19] introduced a protocol, realizable with cold atoms, for purely dissipative dynamics which approaches at a finite rate a mixed steady state as close as desired to a pure topological state. Yet, the resulting topology is encoded in the *Hermitian* steady-state density matrix, giving rise to the same topological classes as in equilibrium [10–12,15,18,21,23–34]. Could this new type of engineered driving still lead to new quantum nonequilibrium criticality?

Every natural system exhibits imperfections and disorder. In equilibrium, it has long been recognized that disorder is actually essential for stabilizing the most basic topological phase, the integer quantum Hall state [35]. Disorder localizes all states in a Landau level except one at energy E_c. The wave-function localization length diverges as one approaches it as [36,37]

$$\xi(E) \sim |E - E_c|^{-\nu}, \tag{1}$$

with a critical exponent ν governing the plateau transition. Lately, a debate arose regarding the theoretical value of ν [38–49], and its relation to experiment [50–52]; the currently accepted value is 2.5–2.6.

In this work we study the interplay between disorder and the recipe of Refs. [18,19] for dissipatively inducing Chern-insulator states, through the effects of disorder on the eigenmodes of the steady-state density matrix, which is experimentally measurable in cold atoms [53–57]. This is thus a Hermitian localization problem, unrelated to disordered non-Hermitian Hamiltonians [58,59]. We show that disorder in the system-bath coupling leads to the same universality class as in equilibrium, while disorder perturbing the system Hamiltonian is not. We employ three different finite-size scaling (FSS) methods, based on (a) the number of conducting states [48,60]; (b) the local Chern marker [61]; and (c) the transfer matrix Lyapunov exponent [37,47]. The final results are presented in Table II; all methods show that the out-of-equilibrium ν is larger by 0.5–0.6 than equilibrium, hinting at a different universality class.

Recipe. We now briefly recall the recipe for the dissipative creation of topological states, which is comprehensively described in Ref. [18]. Suppose we have a "reference Hamiltonian," $H^{\mathrm{ref}} = \sum_{i,j} h_{ij}^{\mathrm{ref}} c_i^\dagger c_j = \sum_\lambda \varepsilon_\lambda^{\mathrm{ref}} c_\lambda^\dagger c_\lambda$ (i, j being real space indexes in two dimensions, and λ an eigenvalue index, which, in the clean case, would correspond to the band number and lattice momentum), with some desired (e.g., topologically nontrivial) gapped ground state where only low-lying states ($\lambda \leqslant \lambda_0$) are filled. Rather than implementing H^{ref} as the system Hamiltonian, one may set the system Hamiltonian to zero and employ dissipation to drive the system into a steady state which is close to the ground state of H^{ref}. For this one takes a system consisting of two types of fermions (e.g., cold-atom hyperfine states), with respective creation operators $a_i^\dagger$ (system) and $b_i^\dagger$ (bath). Both fermion species feel a lattice potential in the xy plane, but the bath b fermions could also escape in the z direction. Besides that, the Hamiltonian of

TABLE I. Methods parameters: W is the disorder strength, L and L_x the system size in the y and x directions, respectively, N_g the grid size (method I), M the number of disorder realizations, $L_x^{\rm eff}$ the effective x length (method III), p the hopping range cutoff (method III, nonequilibrium), $\mu^{\rm eff}$ the effective chemical potential, and $\gamma^{\rm in}/\gamma^0$ the refilling rate in units of $\gamma^0 = 2\pi\nu_0 t^2$.

	Equilibrium							Out of equilibrium								
Method	W	Geometry	L	L_x	N_g	M	$L_x^{\rm eff}$	W	$\mu^{\rm eff}$	$\frac{\gamma^{\rm in}}{\gamma^0}$	Geometry	L	L_x	p	N_g	M	$L_x^{\rm eff}$
I	0.2	$L\times L$	28–63		30	53000–740[a]		2	−3.6	0.2	$L\times L$	35–63			25–31[b]	32000–290[a]	
II	0.2	$L\times L$	21–77			30000		2	−3.6	0.2	$L\times L$	28–77				3000–1500[c]	
III	0.2	$L\times L_x$	14–210	2×10^7		5	10^8	5.5	−3.6	0.2	$L\times L_x$	14–49	105	5		15000	1.3×10^6

[a] M depends on L [62].
[b] $N_g = 25$ for $L \leqslant 49$ and $N_g = 31$ for $L = 56, 63$.
[c] $M = 3000$ for $L \leqslant 63$ and $M = 1500$ for $L = 70, 77$.

the a fermions is trivial, ideally featuring no hopping; deviations from this will be described by a system Hamiltonian $H_S = \sum_{i,j} h_{S,ij} a_i^\dagger a_j$. Rather, the dynamics originates from the system-bath coupling Hamiltonian, which is built out of the matrix elements of the reference Hamiltonian. In the rotating frame (with respect to the system and bath Hamiltonians) it acquires a time-independent form,

$$H_{SB} = \sum_{i,j} \left(h_{ij}^{\rm ref} - \mu^{\rm eff}\delta_{ij}\right) b_i^\dagger a_j + \text{H.c.}$$
$$= \sum_{\lambda} \left(\varepsilon_\lambda^{\rm ref} - \mu^{\rm eff}\right) b_\lambda^\dagger a_\lambda + \text{H.c.}, \qquad (2)$$

where $\mu^{\rm eff}$ is an effective "chemical potential." The utility of the construction now becomes apparent: Suppose the lowest energy band of the reference Hamiltonian is almost flat (dispersionless). By tuning $\mu^{\rm eff}$ to its center ($\varepsilon_\lambda^{\rm ref} \approx \mu^{\rm eff}$ for all $\lambda \leqslant \lambda_0$), its states become *weakly coupled* to the bath compared to states in the other bands, $\lambda > \lambda_0$. Thus, all states are evaporated rapidly, except those belonging to the lowest band. One may then introduce another similar reservoir which refills all trapped states at a uniform rate. Coupling the system to these two reservoirs with different chemical potentials stabilizes a nonequilibrium steady state close to the ground state of the reference Hamiltonian, as we now explain.

Integrating out the baths one gets a Lindblad [63] master equation, from which the Gaussian steady state ρ can be obtained. The latter is completely characterized by the single-particle density matrix $G_{ij} \equiv \text{tr}(\rho a_i^\dagger a_j)$, which obeys a continuous Lyapunov equation [18,19,64]:

$$i[G, h_S^*] + \tfrac{1}{2}\{G, \gamma^{\rm out} + \gamma^{\rm in}\} = \gamma^{\rm in}, \qquad (3)$$

where $\gamma^{\rm in}, \gamma^{\rm out}$ are non-negative Hermitian matrices that describe the rates which particles enter/escape the system, and h_S^* is the complex conjugate of the matrix h_S. By Fermi's golden rule, $\gamma_\lambda^{\rm out} = 2\pi\nu_0(\varepsilon_\lambda^{\rm ref} - \mu^{\rm eff})^2$ is diagonal in the eigenbasis of the reference Hamiltonian [more generally, as a matrix $\gamma^{\rm out} = 2\pi\nu_0(h^{\rm ref} - \mu^{\rm eff}\mathbb{1})^2$], with ν_0 the density of states of the b species (assumed constant), while $\gamma^{\rm in}$ is taken as state independent (proportional to the unit matrix). For $h_S = 0$, we can solve Eq. (3) explicitly:

$$G = \left[1 + \frac{2\pi\nu_0}{\gamma^{\rm in}}(h^{\rm ref} - \mu^{\rm eff}\mathbb{1})^2\right]^{-1}. \qquad (4)$$

We see that G is diagonal in the eigenbasis of $H^{\rm ref}$, with eigenvalues $n_\lambda = \gamma^{\rm in}/(\gamma^{\rm in} + \gamma_\lambda^{\rm out})$ representing their mean occupation. The coupling to two reservoirs with different chemical potentials thus induced a Lorentzian nonequilibrium distribution (in terms of the energies of $H^{\rm ref}$), unlike the equilibrium Fermi-Dirac distribution. G [or, equivalently, the system-bath entanglement Hamiltonian $-\ln(\rho)$] has a similar band structure to $H^{\rm ref}$ (with the highest occupancy band of G corresponding to the lowest energy band of $H^{\rm ref}$), which is amenable to topological classification [10–12,15,18,19,28]. For $\max_{\lambda\leqslant\lambda_0}(\gamma_\lambda^{\rm out}) \ll \gamma^{\rm in} \ll \min_{\lambda>\lambda_0}(\gamma_\lambda^{\rm out})$ we get $n_{\lambda\leqslant\lambda_0} \approx 1$, $n_{\lambda>\lambda_0} \approx 0$, as desired: The steady state is then close to the ground state of $H^{\rm ref}$ at zero temperature, and will therefore have the same topological index. This motivates the study of the eigenmodes of G and their localization properties in the presence of disorder.

Localization transition. This work compares the localization quantum phase transition of two systems. The first is the equilibrium Hofstadter model [65] for the integer quantum Hall effect on a square lattice:

$$H_H = t\sum_{r_x,r_y} e^{2\pi i\alpha r_y} a_{r_x+1,r_y}^\dagger a_{r_x,r_y} + a_{r_x,r_y+1}^\dagger a_{r_x,r_y} + \text{H.c.}, \qquad (5)$$

where we take $t = 1$, $\alpha = 1/7$. The second system is the out-of-equilibrium analog, built using the recipe described above [18,19]: The Hofstadter Hamiltonian (whose lowest band is naturally almost flat) is taken as the *reference* Hamiltonian $H^{\rm ref} = H_H$, while $H_S = 0$. To study the localization phase transition we introduce disorder. In equilibrium we add a term $H_D = \sum_{r_x,r_y} w_{r_x,r_y} a_{r_x,r_y}^\dagger a_{r_x,r_y}$, where $w_{r_x,r_y} \in [-W, W]$ are independent and uniformly

TABLE II. Summary of the results for the critical exponent ν, in and out of equilibrium.

Method	I	II	III
Equilibrium	2.58 ± 0.04	2.26 ± 0.04	2.53 ± 0.03
Nonequilibrium	2.99 ± 0.10	2.91 ± 0.06	Not convergent, higher than equilibrium

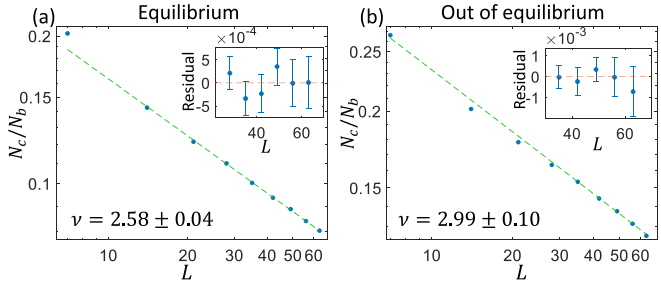

FIG. 1. Log-log plot of $\langle N_c/N_b \rangle$ as a function of L (system size), with N_c the number of conducting states and $N_b = \alpha L^2$ ($\alpha = 1/7$) the total number of states per band. Dashed lines represent linear fits with $L \geqslant 28$ in equilibrium and $L \geqslant 35$ out of equilibrium. Insets: residual plots.

distributed. Out of equilibrium, there are two options for introducing the same disorder term, realizable in cold atoms using the setup introduced in Refs. [18,19]: One may either (a) add H_D to $H^{\rm ref}$ while keeping $H_S = 0$, by adding a random component to the laser beam which drives the on-site $a \to b$ transition in H_{SB}, using, e.g., a speckle pattern [66]; (b) keep $H^{\rm ref} = H_H$ and set $H_S = H_D$, by adding a random component to the optical lattice potential of the a atoms or to the optical potential confining them to the lattice plane. We find that in both cases the disorder causes a nonequilibrium steady-state localization phase transition of the eigenmodes of G. We can define the localization length of an eigenmode of G by the exponential decay of its envelope, in the same way it is defined for the eigenmodes of H in equilibrium [36,37]. Similarly to Eq. (1), it behaves as $\xi(n) \propto |n - n_c|^{-\nu}$, where now it depends on the eigenvalue of G, that is, the occupation n (instead of the energy E). n_c is the critical occupation, which replaces the critical energy E_c. In this work we will concentrate on the band of highest occupation, akin to the lowest Landau band in equilibrium [see, for example, the bottom panel of Fig. 2(b)].

Does ν take the same value as in equilibrium? In the first case the answer is yes; since $H_S = 0$, G is still given by Eq. (4). Thus, even in the presence of disorder, $h^{\rm ref}$ and G share the *same eigenvectors*, hence the same ν [62]. This argument does not hold in the second scenario (disorder in H_S), since G and $h^{\rm ref}$ have different eigenvectors. Here we need to

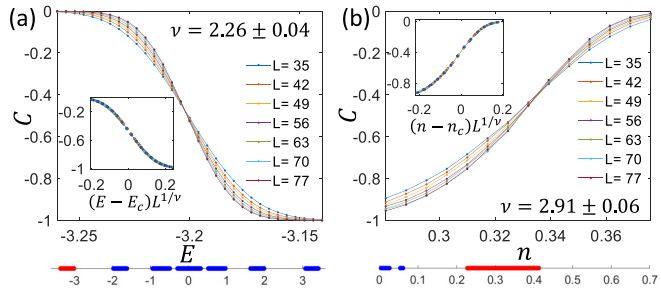

FIG. 2. The average local Chern number (a) in and (b) out of equilibrium. Insets: scaling data collapse. Bottom panels: the seven energy bands in equilibrium, and occupation bands out of equilibrium (note the different scales). The band which is investigated is marked in red and the others in blue.

resort to numerical solution of Eq. (3). We will investigate ν using three FSS methods. For each we first calculate ν in equilibrium (disordered Hofstadter model), and then out of equilibrium ($H^{\rm ref} = H_H$ and $H_S = H_D$). Again, while in equilibrium we examine the properties of the Hamiltonian (e.g., eigenvector localization length, Chern number), out of equilibrium we investigate the same properties, which are now obtained from G instead of the Hamiltonian. While the band structure in equilibrium depends only on α and the disorder strength W, out of equilibrium it also depends on $\gamma^{\rm in}$ and $\mu^{\rm eff}$. The results were found not to be sensitive to their particular values, as long as they are chosen so that the disorder broadens the bands more than their clean width but less than their separation [62]. The parameter values are summarized in Table I, and the final results in Table II.

Method I. Following Ref. [48,62], we calculate the critical exponent in equilibrium by the scaling of the number of conducting states, N_c,

$$N_c(L) \propto L^{2-1/\nu}, \tag{6}$$

where L is the system size and ν is the critical exponent. Working with a $L \times L$ Hofstadter model with periodic boundary conditions, we calculate N_c by counting the number of single-particle states with nonzero Chern number, and average the result over M different disorder realizations. In the presence of disorder, the Chern number can be defined as [67]

$$C_L(\psi) = -\frac{1}{\pi} \int \mathrm{Im} \langle \partial_{\theta_x} \psi | \partial_{\theta_y} \psi \rangle d\theta_x d\theta_y, \tag{7}$$

where $\psi(\theta_x, \theta_y)$ is the single-particle state and the integral is over the space of twisted periodic boundary conditions, defined by the phases $0 \leqslant \theta_x, \theta_y \leqslant 2\pi$. For efficient calculation, we use the method suggested in Ref. [68], employing grid size $N_g \times N_g$ [62]. Corrections to the scaling in Eq. (6) fade quickly with increasing the system size, hence may be ignored by excluding low system sizes. The nonequilibrium generalization is straight-forward: We calculate the Chern number of eigenstates of G (instead of H) by introducing the twisted boundary conditions θ_x, θ_y into $H^{\rm ref}$. Then, we count the conducting states within the highest occupation band. Results are presented in Fig. 1.

Method II. Here we study FSS of the topological index [36,62]. In equilibrium, we define the total Chern number $C_L(E)$ as the sum of the Chern numbers defined in Eq. (7) over all single-particle states ψ with energy below E (hence it varies between 0 when E is below the lowest band, to -1 when it is in the gap between it and the next band). In the vicinity of the critical energy E_c, it scales as

$$C_L(E) = f\big((E - E_c)L^{1/\nu}\big), \tag{8}$$

We note that the transition will be sharp in the thermodynamic limit. For a more efficient estimation of $C_L(E)$, we will use the local Chern marker [61,69] with open boundary conditions,

$$C(r_x, r_y) = -2\pi i \langle r_x, r_y | \tilde{X}\tilde{Y} - \tilde{Y}\tilde{X} | r_x, r_y \rangle, \tag{9}$$

where $\tilde{X}, \tilde{Y}$ are the projected lattice position operators: $\tilde{X} = P(E)XP(E)$, $\tilde{Y} = P(E)YP(E)$, $P(E)$ being a projection onto states with energy below E. The local Chern marker fluctuates around the value of the Chern number in the bulk

of the system, but takes different values on the edges, so that $\sum_{r_x,r_y} C(r_x, r_y) = 0$. Thus, we average $C(r_x, r_y)$ over the bulk, while excluding 1/4 of the sample length from each side, $C_L(E) = (4/L^2) \times \sum_{L/4\leqslant r_x,r_y\leqslant 3L/4} C(r_x, r_y)$, and average the result over M different disorder realizations. As in method I, irrelevant corrections exist, but their influence decreases rapidly with increasing system size. We then search for ν, E_c, and the coefficients of a polynomial approximating f [62], which minimize the chi-squared deviation of $C_L(E)$ from the scaling Eq. (8). Out of equilibrium, we calculate $C_L(n)$, the Chern number of eigenstates of G with occupation *larger* than n, using Eq. (9) with the appropriate projector $P(n)$. The results are presented in Fig. 2.

Method III. Here we perform FSS of the localization length ξ. Following Ref. [70] (see also [62]), we calculate the localization length with the transfer-matrix method: We consider a long cylinder of size $L_x \times L$, $L_x \gg L$. Let ψ be an eigenvalue of the Hamiltonian with energy E. From the equation $H\psi = E\psi$ we can construct the $2L \times 2L$ transfer-matrix T_{r_x}, defined as

$$\begin{pmatrix} \psi_{r_x+1} \\ \psi_{r_x} \end{pmatrix} = T_{r_x} \begin{pmatrix} \psi_{r_x} \\ \psi_{r_x-1} \end{pmatrix}, \tag{10}$$

where ψ_{r_x} is a vector with L elements $\psi_{r_x,r_y=1\cdots L}$. Being symplectic, the eigenvalues of each transfer matrix come in reciprocal pairs $\{\lambda, \lambda^{-1}\}$. The same applies to their product, $\mathcal{T} = \prod_{r_x=1}^{L_x} T_{r_x}$. The Lyapunov exponent (inverse localization length) is defined as

$$\tilde{\Lambda} \equiv \xi^{-1} = \lim_{L_x\to\infty} \frac{\ln(\lambda_{\min})}{L_x}, \tag{11}$$

where $\lambda_{\min}$ is the smallest eigenvalue of $\mathcal{T}$ that is larger than unity. We have applied the Gram-Schmidt process to the columns of $\mathcal{T}$ every seven multiplications to reduce numerical error. The results are presented in Fig. 3(a). As in the previous method, ν can be extracted by finding a function f that minimizes the chi square of the dimensionless Lyapunov exponent $\Lambda \equiv L\tilde{\Lambda}$. However, since the data contains strong corrections to scaling (typical for the long cylinder geometry), we account for a single irrelevant scaling field [62].

The nonequilibrium generalization from $\Lambda(E)$ to $\Lambda(n)$ is more complicated compared to the previous methods. First, unlike H, G has *nonlocal hopping terms* which prevent us from constructing a transfer matrix. This requires introducing a cutoff p on the hopping range in the x direction, and setting terms of range larger than p to zero. From this perspective it is advantageous to construct the transfer matrices using G^{-1}, since Eq. (4) shows that for $H_S = 0$ its elements have a finite range $p = 2$. We have verified numerically that the elements of G^{-1} decay exponentially with range for $H_S = H_D$, making truncation at $p = 5$ a very good approximation [62].

A second issue is that in the presence of disorder the structure of G^{-1} can only be obtained numerically, by solving Eq. (3). Thus, we cannot analytically obtain the transfer matrix at a specific x position, and instead, we can only generate the entire G^{-1} matrix, which is impractical for $L_x \gg 1$. As a solution, we use the scheme depicted in Fig. 3(c): We generate a G^{-1} matrix of size $L_x \times L$ for some large but practical L_x (with periodic boundary conditions) [62]. We repeat this with M disorder realizations, and denote the resulting matrices as $\{(G^{-1})_m\}_{m=1}^{M}$. From each $(G^{-1})_m$ we extract K transfer matrices ($K = L_x - 2c$, excluding the $c = 7$ matrices closest to each end) by imposing a cutoff p on the hopping range, as explained above. We then define the sequence $\{T_n\}_{n=1}^{MK}$, with $T_{(n-1)K+1}, \ldots, T_{nK}$ the transfer matrices extracted from $(G^{-1})_n$. The effective system length is thus $L_{\text{eff}} = MK$. The mismatch between transfer matrices that originate from different G^{-1} (e.g., T_K and T_{K+1}) introduces an error, but it can be reduced by increasing L_x [62].

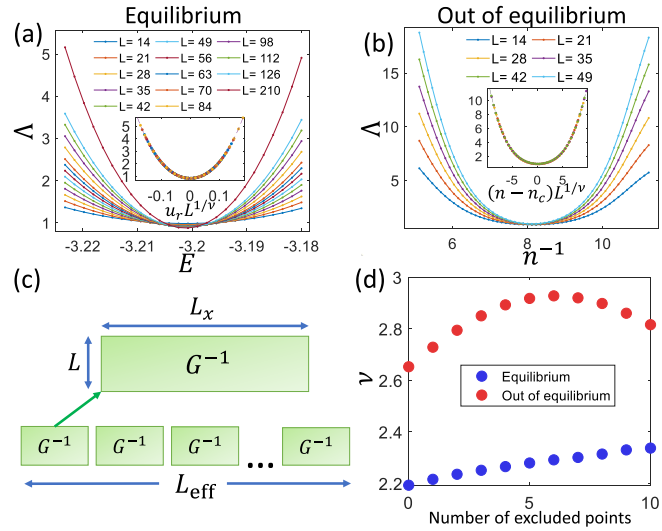

FIG. 3. Dimensionless Lyapunov exponent (a) in and (b) out of equilibrium. Insets: scaling data collapse [in (a) the vertical axis includes corrections to scaling and u_r is the relevant scaling field [62]]. (c) Illustration of the nonequilibrium transfer matrices construction. (d) Comparison of the critical exponent in and out of equilibrium, without corrections to scaling. The horizontal axis represents the number data points that were excluded from each side of the critical point in the chi-squared minimization.

The results are shown in Fig. 3(b). The numerical effort per sample is still much higher in the nonequilibrium case, limiting our ability to reduce statistical error by either sample averaging or using large system sizes. Hence, we can neither implement corrections to scaling nor drop small systems, and therefore cannot determine ν as accurately as before. We thus resort to extracting the uncorrected nonequilibrium exponent and comparing it with a similarly obtained equilibrium value, to appreciate the significance of their difference [see Fig. 3(d)].

Results and discussion. The results are summarized in Table II. In equilibrium they are generally in line with previous studies [38–49]. For method I, the obtained $\nu = 2.58 \pm 0.04$ is somewhat higher than the value $\nu = 2.50 \pm 0.01$ reported in Ref. [48] (also for $\alpha = 1/7$). This might be related to the fact that there the disorder Hamiltonian has been projected to the clean lowest band. In method II, the result ($\nu = 2.26 \pm 0.04$) is smaller than recent estimates of the critical exponent, which seems to be a general feature of FSS of a topological index [46,71]. Let us note that in any case we are interested in the equilibrium-nonequilibrium difference, which is larger than this discrepancy. In method III, upon including corrections to scaling we get $\nu = 2.53 \pm 0.03$,

$y = 0.44 \pm 0.01$, $\Lambda(E_c) = 0.83 \pm 0.01$, with y the leading irrelevant exponent. This is slightly smaller but still in agreement with $\nu = 2.58 \pm 0.03$ obtained in Ref. [47] for the Hofstadter model.

Out of equilibrium, methods I and II give rise to values which are significantly higher than in equilibrium. The results of method III are not convergent, but they still strongly suggest that ν is higher than equilibrium by 0.5–0.6 [see Fig. 3(d)], in agreement with the other methods. We have also verified that our results are insensitive to the specific parameter values [62]. All this points at a different type of nonequilibrium universality class.

Let us reiterate that the single-particle density matrix G is Hermitian. Furthermore, G^{-1} is local in space. The locality is exact for $h_S = 0$, where G^{-1} is essentially the square of h^{ref} [see Eq. (4)]. We have found that for disorder in H_S the elements of G^{-1} have distributions without fat tails, and with averages and correlations which decay exponentially with distance [62]. Thus, our results indicate a different type of universality class of the local Hermitian disordered G^{-1}, which is rooted in the nonequilibrium nature of the system.

The value of ν could be measured experimentally, by using the following protocol: (i) realize the cold-atoms setup described in Ref. [18]; (ii) use a laser speckle [66] to introduce disorder, either in the beam that induces the $a \to b$ transitions (for disorder in H^{ref}), or in the beam that is responsible for the confinement of the a atoms (for disorder in H_S), as discussed above; (iii) measure G as demonstrated in Refs. [53–57]; and (iv) repeat for different system sizes to extract ν through FSS.

Conclusions. In this work we have investigated the effects of disorder on dissipation-induced topological states. We demonstrated the existence of nonequilibrium steady-state localization phase transition similar to the integer quantum Hall plateau transition. Using three FSS methods, we found a significant difference between the value of the critical exponent ν in and out of equilibrium when disorder is introduced into the nondissipative part of the Lindbladian. This indicates a different type of nonequilibrium quantum universality class, despite the steady-state density matrix being Hermitian and local. Our findings could be tested in cold-atom experiments. In the future it would be interesting to investigate other types of disorder (e.g., long range [72–74]), to attack the problem using field theoretical methods [2,37], and to study the relation between the steady state and the non-Hermitian [58,59,75] decay towards it (a relation which is nontrivial out of equilibrium [19]), as well as the possibility of new many-body localization transitions [76,77].

Acknowledgments. We thank I. S. Burmistrov, R. Ilan, and E. Shimshoni for useful discussions. Support by the Israel Science Foundation (Grant No. 227/15) and the US-Israel Binational Science Foundation (Grant No. 2016224) is gratefully acknowledged.

[1] A. Kamenev, *Field Theory of Non-Equilibrium Systems* (Cambridge University Press, Cambridge, UK, 2009).

[2] L. M. Sieberer, M. Buchhold, and S. Diehl, Keldysh field theory for driven open quantum systems, Rep. Prog. Phys. **79**, 096001 (2016).

[3] S. Diehl, A. Micheli, A. Kantian, B. Kraus, H. P. Buchler, and P. Zoller, Quantum states and phases in driven open quantum systems with cold atoms, Nat. Phys. **4**, 878 (2008).

[4] B. Kraus, H. P. Buchler, S. Diehl, A. Kantian, A. Micheli, and P. Zoller, Preparation of entangled states by quantum Markov processes, Phys. Rev. A **78**, 042307 (2008).

[5] F. Verstraete, M. M. Wolf, and J. I. Cirac, Quantum computation and quantum-state engineering driven by dissipation, Nat. Phys. **5**, 633 (2009).

[6] H. Weimer, M. Muller, I. Lesanovsky, P. Zoller, and H. P. Buchler, A Rydberg quantum simulator, Nat. Phys. **6**, 382 (2010).

[7] J. Otterbach and M. Lemeshko, Dissipative Preparation of Spatial Order in Rydberg-Dressed Bose-Einstein Condensates, Phys. Rev. Lett. **113**, 070401 (2014).

[8] N. Lang and H. P. Buchler, Exploring quantum phases by driven dissipation, Phys. Rev. A **92**, 012128 (2015).

[9] L. Zhou, S. Choi, and M. D. Lukin, Symmetry-protected dissipative preparation of matrix product states, arXiv:1706.01995.

[10] S. Diehl, E. Rico, M. A. Baranov, and P. Zoller, Topology by dissipation in atomic quantum wires, Nat. Phys. **7**, 971 (2011).

[11] C.-E. Bardyn, M. A. Baranov, E. Rico, A. İmamoğlu, P. Zoller, and S. Diehl, Majorana Modes in Driven-Dissipative Atomic Superfluids with a Zero Chern Number, Phys. Rev. Lett. **109**, 130402 (2012).

[12] C.-E. Bardyn, M. A. Baranov, C. V. Kraus, E. Rico, A. Imamoglu, P. Zoller, and S. Diehl, Topology by dissipation, New J. Phys. **15**, 085001 (2013).

[13] R. Konig and F. Pastawski, Generating topological order: No speedup by dissipation, Phys. Rev. B **90**, 045101 (2014).

[14] E. Kapit, M. Hafezi, and S. H. Simon, Induced Self-Stabilization in Fractional Quantum Hall States of Light, Phys. Rev. X **4**, 031039 (2014).

[15] J. C. Budich, P. Zoller, and S. Diehl, Dissipative preparation of Chern insulators, Phys. Rev. A **91**, 042117 (2015).

[16] F. Iemini, D. Rossini, R. Fazio, S. Diehl, and L. Mazza, Dissipative topological superconductors in number-conserving systems, Phys. Rev. B **93**, 115113 (2016).

[17] Z. Gong, S. Higashikawa, and M. Ueda, Zeno Hall Effect, Phys. Rev. Lett. **118**, 200401 (2017).

[18] M. Goldstein, Dissipation-induced topological insulators: A no-go theorem and a recipe, SciPost Phys. **7**, 67 (2019).

[19] G. Shavit and M. Goldstein, Topology by dissipation: Transport properties, Phys. Rev. B **101**, 125412 (2020).

[20] F. Tonielli, J. C. Budich, A. Altland, and S. Diehl, Topological Field Theory Far from Equilibrium, Phys. Rev. Lett. **124**, 240404 (2020).

[21] T. Yoshida, K. Kudo, H. Katsura, and Y. Hatsugai, Fate of fractional quantum Hall states in open quantum systems: Characterization of correlated topological states for the full Liouvillian, Phys. Rev. Research **2**, 033428 (2020).

[22] S. Bandyopadhyay and A. Dutta, Dissipative preparation of many-body Floquet Chern insulators, Phys. Rev. B **102**, 184302 (2020).

[23] A. Altland, M. Fleischhauer, and S. Diehl, Symmetry classes of open fermionic quantum matter, Phys. Rev. X **11**, 021037 (2021).
[24] A. Rivas, O. Viyuela, and M. A. Martin-Delgado, Density-matrix Chern insulators: Finite-temperature generalization of topological insulators, Phys. Rev. B **88**, 155141 (2013).
[25] Z. Huang and D. P. Arovas, Topological Indices for Open and Thermal Systems via Uhlmann's Phase, Phys. Rev. Lett. **113**, 076407 (2014).
[26] O. Viyuela, A. Rivas, and M. A. Martin-Delgado, Two-Dimensional Density-Matrix Topological Fermionic Phases: Topological Uhlmann Numbers, Phys. Rev. Lett. **113**, 076408 (2014).
[27] E. P. L. van Nieuwenburg and S. D. Huber, Classification of mixed-state topology in one dimension, Phys. Rev. B **90**, 075141 (2014).
[28] J. C. Budich and S. Diehl, Topology of density matrices, Phys. Rev. B **91**, 165140 (2015).
[29] F. Grusdt, Topological order of mixed states in correlated quantum many-body systems, Phys. Rev. B **95**, 075106 (2017).
[30] C.-E. Bardyn, A recipe for topological observables of density matrices, arXiv:1711.09735.
[31] C.-E. Bardyn, L. Wawer, A. Altland, M. Fleischhauer, and S. Diehl, Probing the Topology of Density mMatrices, Phys. Rev. X **8**, 011035 (2018).
[32] D.-J. Zhang and J. Gong, Topological characterization of one-dimensional open fermionic systems, Phys. Rev. A **98**, 052101 (2018).
[33] A. Coser and D. Pérez-García, Classification of phases for mixed states via fast dissipative evolution, Quantum **3**, 174 (2019).
[34] S. Lieu, M. McGinley, and N. R. Cooper, Tenfold Way for Quadratic Lindbladians, Phys. Rev. Lett. **124**, 040401 (2020).
[35] K. v. Klitzing, G. Dorda, and M. Pepper, New Method for High-Accuracy Determination of the Fine-Structure Constant Based on Quantized Hall Resistance, Phys. Rev. Lett. **45**, 494 (1980).
[36] B. Huckestein, Scaling theory of the integer quantum Hall effect, Rev. Mod. Phys. **67**, 357 (1995).
[37] F. Evers and A. D. Mirlin, Anderson transitions, Rev. Mod. Phys. **80**, 1355 (2008).
[38] K. Slevin and T. Ohtsuki, Critical exponent for the quantum Hall transition, Phys. Rev. B **80**, 041304(R) (2009).
[39] H. Obuse, A. R. Subramaniam, A. Furusaki, I. A. Gruzberg, and A. W. W. Ludwig, Conformal invariance, multifractality, and finite-size scaling at Anderson localization transitions in two dimensions, Phys. Rev. B **82**, 035309 (2010).
[40] M. Amado, A. V. Malyshev, A. Sedrakyan, and F. Domínguez-Adame, Numerical Study of the Localization Length Critical Index in a Network Model of Plateau-Plateau Transitions in the Quantum Hall Effect, Phys. Rev. Lett. **107**, 066402 (2011).
[41] I. C. Fulga, F. Hassler, A. R. Akhmerov, and C. W. J. Beenakker, Topological quantum number and critical exponent from conductance fluctuations at the quantum Hall plateau transition, Phys. Rev. B **84**, 245447 (2011).
[42] K. Slevin and T. Ohtsuki, Finite size scaling of the Chalker-Coddington model, Int. J. Mod. Phys.: Conf. Ser. **11**, 60 (2012).
[43] H. Obuse, I. A. Gruzberg, and F. Evers, Finite-Size Effects and Irrelevant Corrections to Scaling Near the Integer Quantum Hall Transition, Phys. Rev. Lett. **109**, 206804 (2012).
[44] W. Nuding, A. Klumper, and A. Sedrakyan, Localization length index and subleading corrections in a Chalker-Coddington model: A numerical study, Phys. Rev. B **91**, 115107 (2015).
[45] I. A. Gruzberg, A. Klumper, W. Nuding, and A. Sedrakyan, Geometrically disordered network models, quenched quantum gravity, and critical behavior at quantum Hall plateau transitions, Phys. Rev. B **95**, 125414 (2017).
[46] M. Ippoliti, S. D. Geraedts, and R. N. Bhatt, Integer quantum Hall transition in a fraction of a Landau level, Phys. Rev. B **97**, 014205 (2018).
[47] M. Puschmann, P. Cain, M. Schreiber, and T. Vojta, Integer quantum Hall transition on a tight-binding lattice, Phys. Rev. B **99**, 121301(R) (2019).
[48] Q. Zhu, P. Wu, R. N. Bhatt, and X. Wan, Localization-length exponent in two models of quantum Hall plateau transitions, Phys. Rev. B **99**, 024205 (2019).
[49] B. Sbierski, E. J. Dresselhaus, J. E. Moore, and I. A. Gruzberg, Criticality of Two-Dimensional Disordered Dirac Fermions in the Unitary Class and Universality of the Integer Quantum Hall Transition, Phys. Rev. Lett. **126**, 076801 (2021).
[50] W. Li, G. A. Csáthy, D. C. Tsui, L. N. Pfeiffer, and K. W. West, Scaling and Universality of Integer Quantum Hall Plateau-to-Plateau Transitions, Phys. Rev. Lett. **94**, 206807 (2005).
[51] W. Li, C. L. Vicente, J. S. Xia, W. Pan, D. C. Tsui, L. N. Pfeiffer, and K. W. West, Scaling in Plateau-to-Plateau Transition: A Direct Connection of Quantum Hall Systems with the Anderson Localization Model, Phys. Rev. Lett. **102**, 216801 (2009).
[52] A. J. M. Giesbers, U. Zeitler, L. A. Ponomarenko, R. Yang, K. S. Novoselov, A. K. Geim, and J. C. Maan, Scaling of the quantum Hall plateau-plateau transition in graphene, Phys. Rev. B **80**, 241411(R) (2009).
[53] P. Hauke, M. Lewenstein, and A. Eckardt, Tomography of Band Insulators from Quench Dynamics, Phys. Rev. Lett. **113**, 045303 (2014).
[54] N. Fläschner, B. S. Rem, M. Tarnowski, D. Vogel, D.-S. Lühmann, K. Sengstock, and C. Weitenberg, Experimental reconstruction of the Berry curvature in a Floquet Bloch band, Science **352**, 1091 (2016).
[55] M. Tarnowski, M. Nuske, N. Fläschner, B. Rem, D. Vogel, L. Freystatzky, K. Sengstock, L. Mathey, and C. Weitenberg, Observation of Topological Bloch-State Defects and their Merging Transition, Phys. Rev. Lett. **118**, 240403 (2017).
[56] L. A. Peña Ardila, M. Heyl, and A. Eckardt, Measuring the Single-Particle Density Matrix for Fermions and Hard-Core Bosons in an Optical Lattice, Phys. Rev. Lett. **121**, 260401 (2018).
[57] J.-H. Zheng, B. Irsigler, L. Jiang, C. Weitenberg, and W. Hofstetter, Measuring an interaction-induced topological phase transition via the single-particle density matrix, Phys. Rev. A **101**, 013631 (2020).
[58] N. Hatano and D. R. Nelson, Localization Transitions in Non-Hermitian Quantum Mechanics, Phys. Rev. Lett. **77**, 570 (1996).
[59] Y. Ashida, Z. Gong, and M. Ueda, Non-Hermitian physics, Adv. Phys. **69**, 249 (2020).
[60] K. Yang and R. N. Bhatt, Floating of Extended States and Localization Transition in a Weak Magnetic Field, Phys. Rev. Lett. **76**, 1316 (1996).

[61] R. Bianco and R. Resta, Mapping topological order in coordinate space, Phys. Rev. B **84**, 241106(R) (2011).

[62] See Supplmental Material at http://link.aps.org/supplemental/10.1103/PhysRevB.103.L241401 for technical details.

[63] P. Z. Crispin Gardiner, *Quantum Noise* (Springer, Berlin, Heidelberg, 2004).

[64] F. Schwarz, M. Goldstein, A. Dorda, E. Arrigoni, A. Weichselbaum, and J. von Delft, Lindblad-driven discretized leads for nonequilibrium steady-state transport in quantum impurity models: Recovering the continuum limit, Phys. Rev. B **94**, 155142 (2016).

[65] D. R. Hofstadter, Energy levels and wave functions of Bloch electrons in rational and irrational magnetic fields, Phys. Rev. B **14**, 2239 (1976).

[66] J. Goodman, *Speckle Phenomena in Optics: Theory and Applications* (SPIE, Bellingham, Washington, 2020).

[67] Q. Niu, D. J. Thouless, and Y.-S. Wu, Quantized Hall conductance as a topological invariant, Phys. Rev. B **31**, 3372 (1985).

[68] T. Fukui, Y. Hatsugai, and H. Suzuki, Chern numbers in discretized Brillouin zone: Efficient method of computing (spin) Hall conductances, J. Phys. Soc. Jpn. **74**, 1674 (2005).

[69] M. D. Caio, G. Moller, N. R. Cooper, and M. J. Bhaseen, Topological marker currents in Chern insulators, Nat. Phys. **15**, 257 (2019).

[70] A. MacKinnon and B. Kramer, The scaling theory of electrons in disordered solids: Additional numerical results, Z. Phys. B: Condens. Matter **53**, 1 (1983).

[71] T. A. Loring and M. B. Hastings, Disordered topological insulators via C*-algebras, Europhys. Lett. **92**, 67004 (2010).

[72] M. M. Fogler, A. Y. Dobin, and B. I. Shklovskii, Localization length at the resistivity minima of the quantum Hall effect, Phys. Rev. B **57**, 4614 (1998).

[73] P. M. Ostrovsky, I. V. Gornyi, and A. D. Mirlin, Quantum Criticality and Minimal Conductivity in Graphene with Long-Range Disorder, Phys. Rev. Lett. **98**, 256801 (2007).

[74] A. Rycerz, J. Tworzydło, and C. W. J. Beenakker, Anomalously large conductance fluctuations in weakly disordered graphene, Europhys. Lett. **79**, 57003 (2007).

[75] N. Silberstein, J. Behrends, M. Goldstein, and R. Ilan, Berry connection induced anomalous wave-packet dynamics in non-Hermitian systems, Phys. Rev. B **102**, 245147 (2020).

[76] R. Nandkishore and D. A. Huse, Many-body localization and thermalization in quantum statistical mechanics, Annu. Rev. Condens. Matter Phys. **6**, 15 (2015).

[77] E. Altman and R. Vosk, Universal dynamics and renormalization in many-body-localized systems, Annu. Rev. Condens. Matter Phys. **6**, 383 (2015).